Electron. Mater. Lett., Vol. 10, No. 4 (2014), pp. 719-730
DOI: 10.1007/s13391-013-3270-4

Multifractal Characterization of Water Soluble Copper Phthalocyanine Based Films Surfaces

Ştefan Ţălu,[1] Sebastian Stach,[2] Aman Mahajan,[3] Dinesh Pathak,[4,*] Tomas Wagner,[4] Anshul Kumar,[3] R. K. Bedi,[3] and Mihai Ţălu[5]

[1]Technical University of Cluj-Napoca, Faculty of Mechanical Engineering, Department of AET, Discipline of Descriptive Geometry and Engineering Graphics, 103-105 B-dul Muncii St., Cluj-Napoca 400641, Cluj, Romania
[2]University of Silesia, Faculty of Computer Science and Materials Science, Institute of Informatics, Department of Biomedical Computer Systems, Będzińska 39, 41-205 Sosnowiec, Poland
[3]Guru Nanak Dev University, Department of Physics, Material Science Research Laboratory, Amritsar, 143005, India
[4]University of Pardubice, Faculty of Chemical Technology, Department of General and Inorganic Chemistry, Pardubice, Studentska 573, Pardubice 532 10, Czech Republic
[5]University of Craiova, Faculty of Mechanical Engineering, Department of Applied Mechanics, Calea Bucureşti St., no. 165, Craiova, 200585, Dolj, Romania

(received date: 15 September 2013 / accepted date: 11 November 2013 / published date: 10 July 2014)

This paper presents a multifractal approach to characterize the structural complexity of 3D surface roughness of CuTsPc films on the glass and quartz substrate, obtained with atomic force microscopy (AFM) analysis. CuTsPc films prepared by drop cast method were investigated. CuTsPc films surface roughness was studied by AFM in tapping-mode™, in an aqueous environment, on square areas of 100 μm^2 and 2500 μm^2. A detailed methodology for CuTsPc films surface multifractal characterization, which may be applied for AFM data, was also presented. Analysis of surface roughness revealed that CuTsPc films have a multifractal geometry at various magnifications. The generalized dimension D_q and the singularity spectrum $f(\alpha)$ provided quantitative values that characterize the local scale properties of CuTsPc films surface morphology at nanometer scale. Multifractal analysis provides different yet complementary information to that offered by traditional surface statistical parameters.

Keywords: organic semiconductors, CuTsPc films, atomic force microscopy, multifractal analysis, surface roughness

1. INTRODUCTION

Organic semiconductors are extensively studied for their applications in electrical and optical devices such as organic solar cells, organic thin film transistors and organic light emitting diode.[1-3] Phthalocyanine are small organic molecules characterized by their high symmetry, planarity, electron delocalization and are used as an active layer for electronic devices.[4-6] Metallo phthalocyanine (MPcs) are different class of molecular semiconductor with good thermal and environmental stability, excellent molecular and electronic tunability and also high absorption coefficient.[7-10] Nowadays, the solution processed molecular semiconductors have attracted much attention due to their potential use for low cost device manufacturing. Among them CuTsPc is an emerging material having structure similar to copper phthalocyanine except that polar SO_3Na group is attached to corner benzene ring which make this compound water soluble.[11,12] Recently highly efficient solar cells and gas sensors have been fabricated by using CuTsPc molecule.[13] It has been reported that sulphonated metal phthalocyanine has got enhanced solubility and mobility (1.08 $cm^2v^{-1}s^{-1}$) compared to their non-sulphonated counterpart.[14] In contrast to most solution processed molecular semiconductors, CuTsPc can be deposited from aqueous solution, which simplifies the device fabrication process and makes it potentially more economically as well as ecologically attractive. CuTsPc has also demonstrated potential for more general applications in organic electronics, with new thin film structures being produced for electrode modification as well as template porous and composite structures.[15-17]

The electrical, optical, structural and surface morphological studies of several phthalocyanine thin films have been investigated in recent years,[18-22] however literature on CuTsPc materials is still scant. The quality of materials surface morphology is increasingly important in product multi-performance simulation. In the modern approach from

*Corresponding author: Dineshpathak80@gmail.com

material science, micro and nano structure of materials can be characterized properly using quantitative descriptions. Quantitative description methods may be classified according to Euclidean geometry and fractal/multifractal geometry. The fundamental methods in the conventional quantitative descriptions of the microstructures of materials are statistics, stereology and topology.[23] Euclidean geometrical methods address mainly the measurements of regular objects which are differentiable while fractal/multifractal geometry attempts to solve problems involving the measurements of irregular objects which are self-similar or self-affine. Fractal/multifractal geometry becomes the mathematical fundamental of the quantitative description of irregular microstructures.[23-25] The topography of thin films surfaces add a new level of understanding to the nanotribology processes, such as adhesion, contact formation, friction of adsorbed layers, seen on a atomic level etc. Also, there is a need for atomic-scale methods in thin films surfaces investigation and to try to link atomic-scale observations with macroscopic continuum models and experimental results, particularly concerning structure, energetics, dynamics, transport and thermodynamics processes.

The quantitative characterization of surface morphology of phthalocyanine thin films is important since many physical and chemical properties, such as electrical, optical, and tribological properties depend on the surface morphology.[18-21]

In this study, our particular aspect relates to improving material characterization of 3D surface roughness of CuTsPc films on the glass and quartz substrate, prepared by drop cast method, through atomic force microscopy (AFM) and multifractal analysis. The multifractal analysis reveals the existence of self-similar and multifractal characteristics in the CuTsPc films on the glass and quartz substrate.

1.1 Multifractal analysis

Conventionally, a 3D rough surface analysis is assumed to be a random process, to exhibit fractal characteristics, which can be characterized by fractal parameters that are independent of all scale of roughness.[26,27] The 3D surface topography of thin films possess only statistical self-similarity, which takes place only in the restricted range of the spatial scales.[24] Fractal dimension D_f is a quantitative parameter of a fractal object and describes how the fractal object occupies the metric space to which it belongs. In the case of 3D surfaces, the fractal dimension indicates how much the fractal surface fills the 3D volume.[26-28] Generally, the fractal dimension D_f of a surface is a non-integer value within the range $2 \le D_f \le 3$, where $D_f = 2$ (for ideally smooth surfaces) and $D_f = 3$ (for surfaces with a rough that occupy all available volume).[29] An increasing value of D_f indicate higher level of fractality, a more irregular shape of the surface roughness. In addition, the fractal surface maintains the characteristics of continuity, nondifferentiability and self-similarity of the structure. Different studies suggested a correlation between the different surface roughness parameters and the fractal dimension D_f.[30] However, the surfaces of thin films are geometrically complex and a simple estimation with a single D_f value is not sufficient for predicting thin films topography because it does not offer information about the concentration and distribution of asperities with different orders of size.[31] A more detailed description of 3D surface roughness in order to reflect the heterogeneity of the surface of thin films, both locally and globally, can be obtained by applying multifractal analysis.[24,25] The multifractal structure is characterized by a continuous spectrum of fractal dimensions. A fracture is characterized primarily by a single number, the fractal dimension, while a multifracture is characterized primarily by a function. Thus, a fractal may be interpreted as a special case of a multifractal in which all generalized dimensions are equal to the fractal dimension.[28,32] A thin film surface is covered by nanoasperities (nanoscale protrusions and cavities having different geometries) with different orders of size. The distribution of nanoasperities may spread over a region in such a way that small nanoasperities appear almost everywhere, medium nanoasperities exist in many places, and large nanoasperities are concentrated only in a few places. Multifractal measures are related to the study of the distribution of the concentration of asperities with different orders of size on a surface.[33] Using the computer algorithms,[34,35] multifractal analysis can be applied by means of the quasi-3D[36] and 3D[37,38] methods with reference to the stereometric files of the thin film surfaces. The measurements of the surface were made with the highest possible accuracy in order to meet the criterion of a limit within which the "box" size in the box-counting method approaches zero. Having information about the number of pixels of a profile's binary image covered by individual boxes, it is possible to determine the probability of finding them in a given box,[34] which constitutes the measure of the analyzed set:

$$P_i(r) = L_i(r)/L_T(r) \tag{1}$$

where L_i - number of pixels in one box in the given scale r, L_T - total number of pixels in all boxes in the given scale r, r - box size in the given scale. Multifractal measures can be characterized by the generalized fractal dimensions function $D(q, r)$ (also called the fractal spectrum dimensions for a given set) as:[34]

$$D(q,r) = \frac{1}{q-1}\lim_{r\to 0}\frac{\log\sum_{i=1}^{n}[P_i(r)]^q}{\log r} \tag{2}$$

where q is a number from the range $-\infty$ to $+\infty$. Furthermore, q represents a selective parameter: high values of q enhance cells with relatively high values for P_i; while low values of q

favour cells with relatively low values of P_i. For the particular case where $q = 1$, Eq. (2) becomes indeterminate, so $D(q, r)$ is estimated by l'Hôpital's rule. The generalized dimensions, D_q for $q = 0$, $q = 1$ and $q = 2$, are known as the capacity (or box-counting), the information (or Shannon) entropy and correlation dimensions, respectively. D_0 is the classical fractal dimension that provides average information on the geometric support of the measure. D_1 quantifies the degree of disorder present in a distribution. D_2 is mathematically associated with the correlation function and measures the mean distribution density of the statistical measure. D_q is a monotonically decreasing function of q. All dimensions are different, satisfying $D_0 > D_1 > D_2$. The limits of the generalized dimension spectrum are $D_{-\infty}$ and D_{∞}.

Another way of presenting the multifractal measures description is spectrum $f(\alpha)$. Based on the probability values defined by Eq. (1), a one-parameter family of normalized measures is constructed:

$$\mu(q,r) = [P_i(r)]^q \Big/ \sum_{i=1}^{n} [P_i(r)]^q \tag{3}$$

where $\sum_{i=1}^{n} [P_i(r)]^q$ indicates the summation with q exponent order of the probability for all boxes.

The fractal dimensions of the subset $f(q, r)$ are determined:

$$f(q,r) = \lim_{r \to 0} \frac{\sum_{i=1}^{n} \mu_i(q,r) \log \mu_i(q,r)}{\log r} \tag{4}$$

indexed with the exponents $\alpha(q, r)$:

$$\alpha(q,r) = \lim_{r \to 0} \frac{\sum_{i=1}^{n} \mu_i(q,r) \log P_i(q,r)}{\log r}. \tag{5}$$

The values obtained $\alpha(q, r)$ are called the singularity for the given set. The plot $f(\alpha)$ is called a multifractal spectrum, which presents the whole spectrum of fractal dimensions.

Some of its general properties are as follows: a) curve $f(\alpha)$ is convex with a single inflection point at the maximum with $q = 0$; b) for $q = \pm\infty$, the slope is infinite and $\alpha_{\min} = D_{+\infty}$, $\alpha_{\max} = D_{-\infty}$; c) the spacing of the multifractal spectrum's arms is a measure of the non-homogeneity of the set analyzed; d) where the arms' spacing equals zero (i.e., where the analyzed spectrum is reduced to a point), a fractal case takes place, for which one fractal dimension can be determined. The spectrum width or degree of multifractality is defined as $\Delta\alpha = \alpha_{\max} - \alpha_{\min}$.

The spectrum arms' height difference is defined as: $\Delta f = f(\alpha_{\min}) - f(\alpha_{\max})$. If $\Delta f < 0$ the fragments described by the low probability value predominate; whereas, for $\Delta f > 0$ the fragments described by the high probability value predominate. The left arm of the multifractal spectrum corresponds to strongly irregular areas, defined by a high dimension value; whereas, the right arm of the multifractal spectrum is associated with flat areas, being characteristic for large convex and concave surfaces.[39]

In order to present an image as a three-dimensional surface, it is necessary to replace grey points with local maxima.[34] Fractal/multifractal analysis of a grayscale image gives the fractal dimension $D_0 = 2.0$. Of course, such an analysis may seem to be pointless, since the dimension will be equal to 2 for each analysed image. However, it should be emphasized that the multifractal spectrum in multifractal analysis carries relevant information.

In our study, the multifractal analyses depend on the experimental and methodological parameters involved in AFM measurements, such as: measurement system, diversity of samples, image acquisition, type of image, image processing, multifractal analysis methods, including the algorithm and specific calculation used, etc.[32]

2. MATERIALS AND METHODS

2.1 Materials

The sulphonated copper phthalocyanine was obtained from Sigma-Aldrich Inc. (Aldrich, 85%) and used without further purification. Its molecular structure is shown in Fig. 1.

Before starting the deposition glass and quartz substrate were cleaned in ultrasonic bath for 10 minute using acetone, followed by rinsing in distilled water. Solution was prepared using deionised water and basic solution (0.1 M NH_3, ph11) with the CuTsPc concentration ranging from 5 to 20 mg per ml. The solution was stirred for 24 h at 50°C and then filtered (0.2 μm filter) before being drop cast in air at ambient conditions. The films were dried for 30 minute in air at room temperature, followed by heating for 15 min at 100°C under an inert atmosphere to remove any remaining water and ammonia.

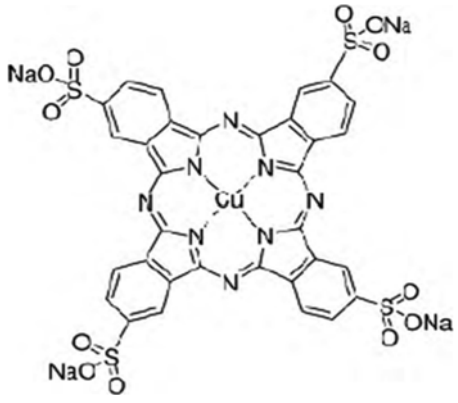

Fig. 1. The chemical structure of sulphonated copper-phthalocyanine (CuTsPc).

2.2 Experimental methods

The structural properties of CuTsPc films were investigated by means of XRD scan taken using CuK_{α} (wavelength = 1.5405 Å) by Bruker diffractometer. The surface morphology of CuTsPc films was determined using a Nanosurf Easyscan 2 AFM system[41] operating in contact mode and in static force. The experiments were done in the same room, at room temperature (23 ± 1°C) and (50 ± 1%) relative humidity. AFM analysis was performed, on areas of 10 to 50 μm^2, using a Model CL-10 cantilever (Vista Probes Cantilever, USA),[42] a pyramidal-shaped silicon cantilever with the following nominal specifications: resonant frequency 12 kHz, spring constant 0.2 N/m, radius 2 nm, length 450 μm, width 40 μm and thickness 2 μm was used. All samples were acquired at a scan rate of 1 Hz with a 256 × 256 pixels image definition over different square areas. The measurements were repeated four times for each sample on different reference areas, to validate the reproducibility of these features. AFM images were analyzed using scanning probe image processor (SPIP) software.[43] The multifractal analyses from the AFM data were made using the proposed multifractal analysis method.

2.3 Design of experiments and statistical analysis method

Detailed surface characterization of the thin films was obtained using six quantitative parameters [height, functional, spatial, hybrid, functional (volume) and feature parameters], according with ISO 25178-2: 2012,[40] provided by the AFM software. Detailed information on the objective parameters used to obtain data on the surface roughness of the thin films, are reported in the appendix. In our study, the statistical description and the multifractal geometry is used to characterize the thin films 3D surface roughness. Statistical analyses were performed using the GraphPad InStat version 3.20 computer software package (GraphPad, San Diego, CA, USA).[26] The Kolmogorov-Smirnov test was used to assess the normal distribution of quantitative variables. Comparisons among different areas within the same sample were performed using independent samples T-test. When statistical significance was found, the difference between two groups was further compared using the Mann-Whitney U test. Differences with a P value of 0.05 or less were considered statistically significant. The average D_q results were expressed as mean value and standard deviation.

3. RESULTS

An analysis of the stereometric files was conducted based on the original algorithm (in MATLAB software R2012b, MathWorks, Inc.), which consists in fractal scaling (in many approximation steps) of the surface measured with an AFM. The representative 3D topographic images of the CuTsPc films deposited on quartz and glass substrate, for scanning square area of 10 μm × 10 μm and 50 μm × 50 μm are shown in Fig. 2(a) & (b) and Fig. 3(a) & (b).

The depth histogram associated with Figs. 2 & 3, are shown in Figs. 4 & 5.

Details of the volume parameters (surface): *Vmp*, *Vvc*, *Vmc* & *Vvv* parameters used to obtain information about the surface morphology (Fig. 6, Fig. 7) are given in the Appendix.

The curve of the material share provides important information about the condition of the surface in terms of its operational suitability. It is known that for the optimal functionality of the surface, it is required to be progressive or progressive-regressive.

The curves (Fig. 6 and Fig. 7) are degressive-progressive. Therefore, it was necessary to determine the linearization of the curves (Fig. 8 and Fig. 9). The designated intersection lines made it possible to determine the share of the load bearing capacity of the material peaks *Sr1* and pits *Sr2*.

The peak count histogram associated with Figs. 2 & 3, are shown in Figs. 10 & 11.

The multifractal singularity spectrum $f(\alpha)$ for scanning

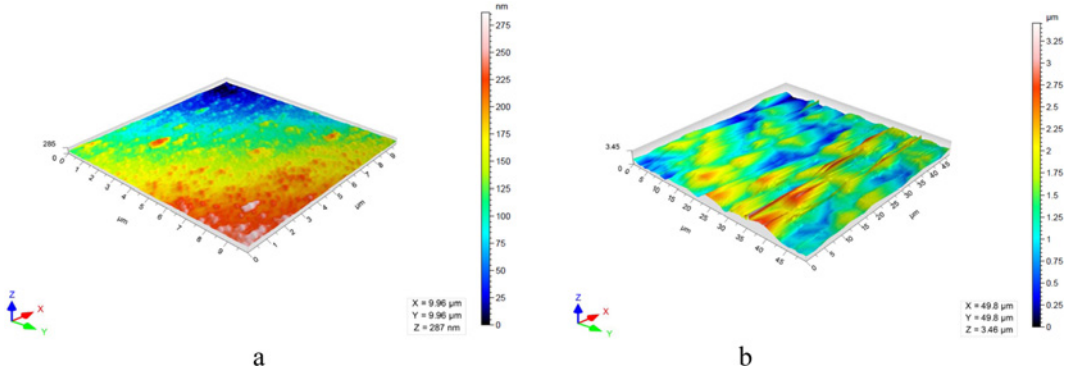

Fig. 2. A representative AFM image of the CuTsPc films deposited on quartz substrate. Microtopographic 3D perspective image. a) Scanning square area of 10 μm × 10 μm. b) Scanning square area of 50 μm × 50 μm. The vertical range of the displayed data (a - in nanometres [nm], b - in micrometers [μm]) and the colour bar are shown on the right side of the AFM image.

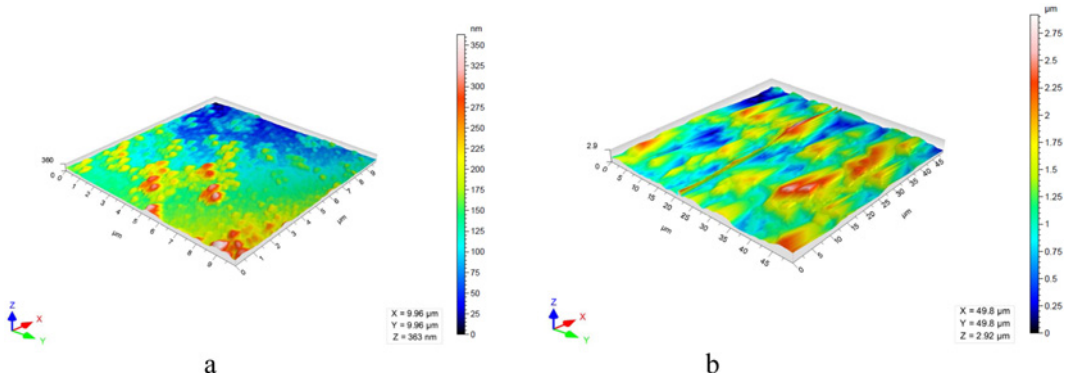

Fig. 3. A representative AFM image of the CuTsPc films deposited on glass substrate. Microtopographic 3D perspective image. a) Scanning square area of 10 μm × 10 μm. b) Scanning square area of 50 μm × 50 μm. The vertical range of the displayed data (a - in nanometres [nm], b - in micrometers [μm]) and the colour bar are shown on the right side of the AFM image.

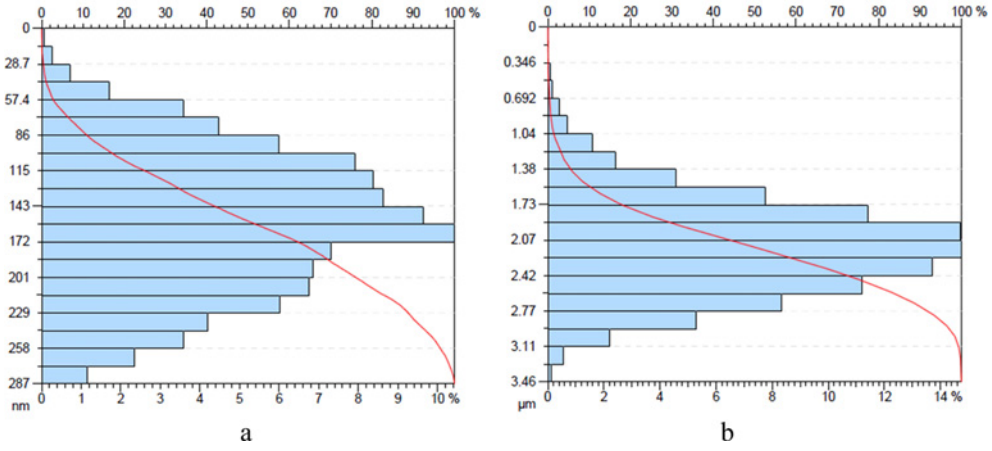

Fig. 4. The depth histogram enables to observe the density of the distribution of the data points on the surface. The vertical axis is graduated in depths: the horizontal axis is graduated in % of the whole population. The Abbott-Firestone curve presents the bearing ratio curve, i.e. for a given depth, the percentage of the material traversed in relation to the area covered. This function is the cumulating function of the amplitude distribution function. The horizontal axis represents the bearing ratio (in %), and the vertical axis represents the depths (in the measurement unit). The CuTsPc films deposited on quartz substrate. a) Scanning square area of 10 μm × 10 μm. b) Scanning square area of 50 μm × 50 μm.

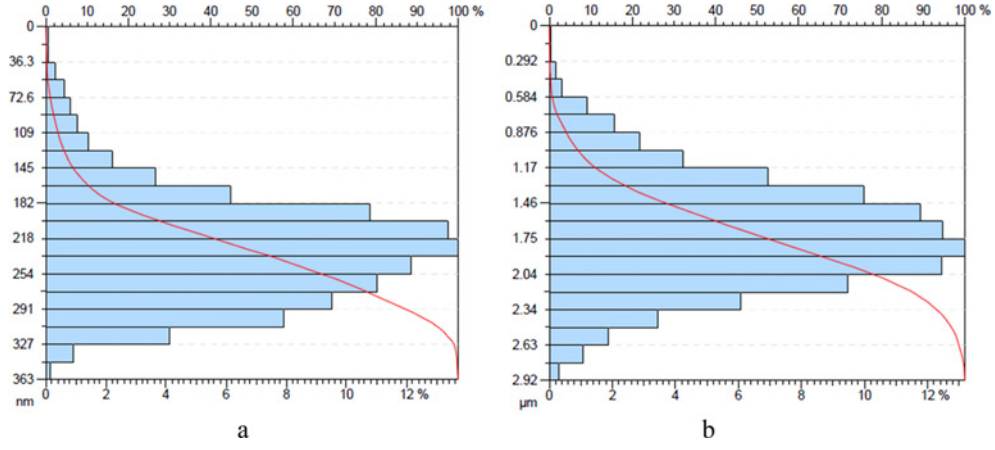

Fig. 5. The depth histogram enables to observe the density of the distribution of the data points on the surface. The vertical axis is graduated in depths: the horizontal axis is graduated in % of the whole population. The Abbott-Firestone curve presents the bearing ratio curve, i.e. for a given depth, the percentage of the material traversed in relation to the area covered. This function is the cumulating function of the amplitude distribution function. The horizontal axis represents the bearing ratio (in %), and the vertical axis represents the depths (in the measurement unit). The CuTsPc films deposited on glass substrate. a) Scanning square area of 10 μm × 10 μm. b) Scanning square area of 50 μm × 50 μm.

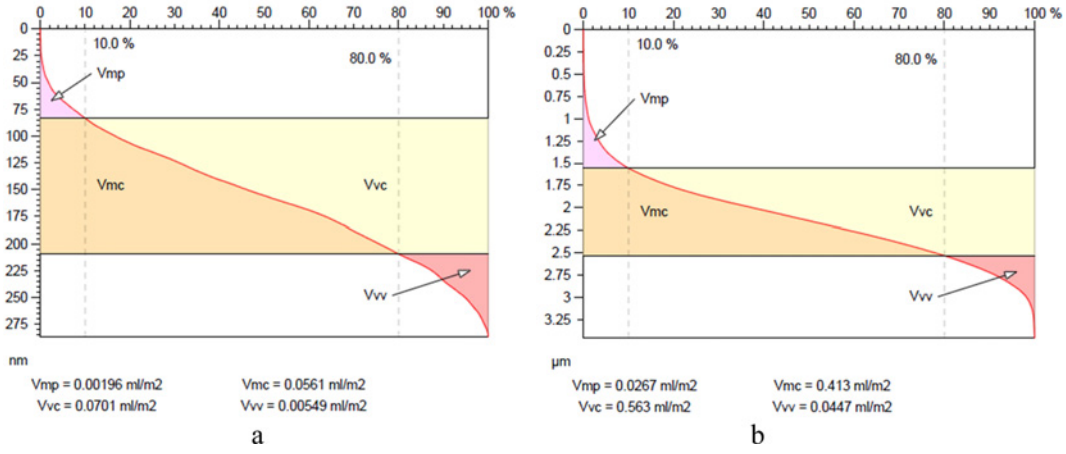

Fig. 6. Graphical study of volume parameters (surface): *Vmp*, *Vvc*, *Vmc* & *Vvv* parameters based upon the Abbott curve calculated on the surface. Two bearing ratio thresholds are defined (using the vertical bars that are drawn with dotted lines). By default, these thresholds are set at bearing ratios of 10% and 80%. The first threshold, *p1* (default: 10%), is used to define the cut level *c1* (and *p2* defines *c2*, respectively). The CuTsPc films deposited on quartz substrate. a) Scanning square area of 10 μm × 10 μm. b) Scanning square area of 50 μm × 50 μm.

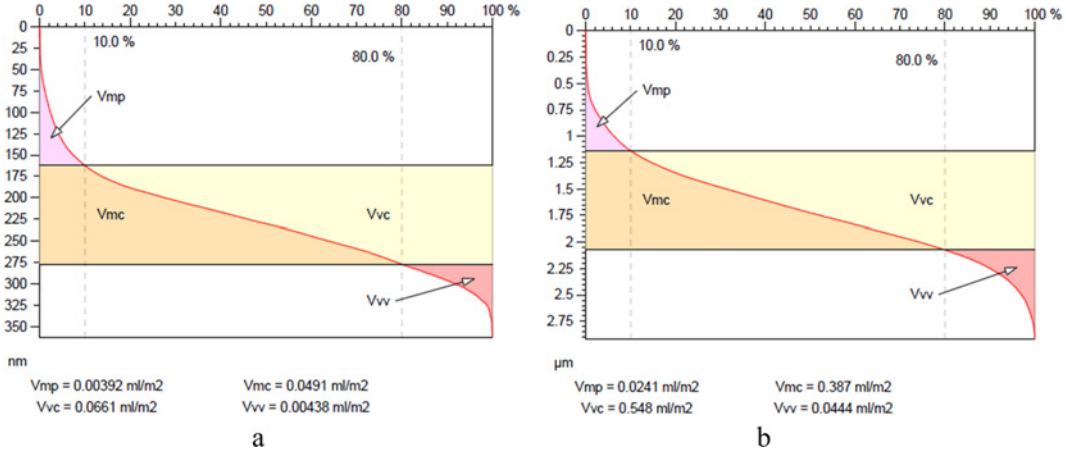

Fig. 7. Graphical study of volume parameters (surface): *Vmp*, *Vvc*, *Vmc* & *Vvv* parameters based upon the Abbott curve calculated on the surface. Two bearing ratio thresholds are defined (using the vertical bars that are drawn with dotted lines). By default, these thresholds are set at bearing ratios of 10% and 80%. The first threshold, *p1* (default: 10%), is used to define the cut level *c1* (and *p2* defines *c2*, respectively). The CuTsPc films deposited on glass substrate. a) Scanning square area of 10 μm × 10 μm. b) Scanning square area of 50 μm × 50 μm.

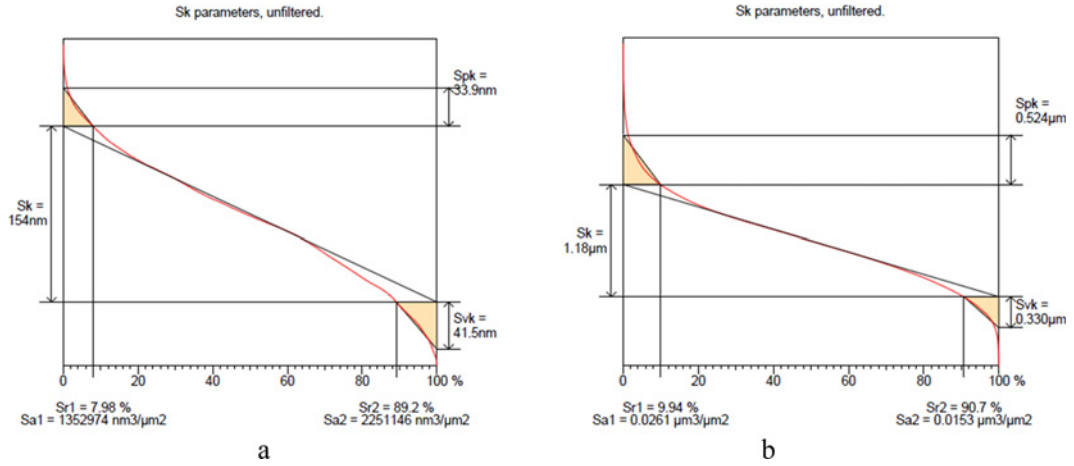

Fig. 8. Graphical study of Sk parameters. The CuTsPc films deposited on quartz substrate. a) Scanning square area of 10 μm × 10 μm. b) Scanning square area of 50 μm × 50 μm.

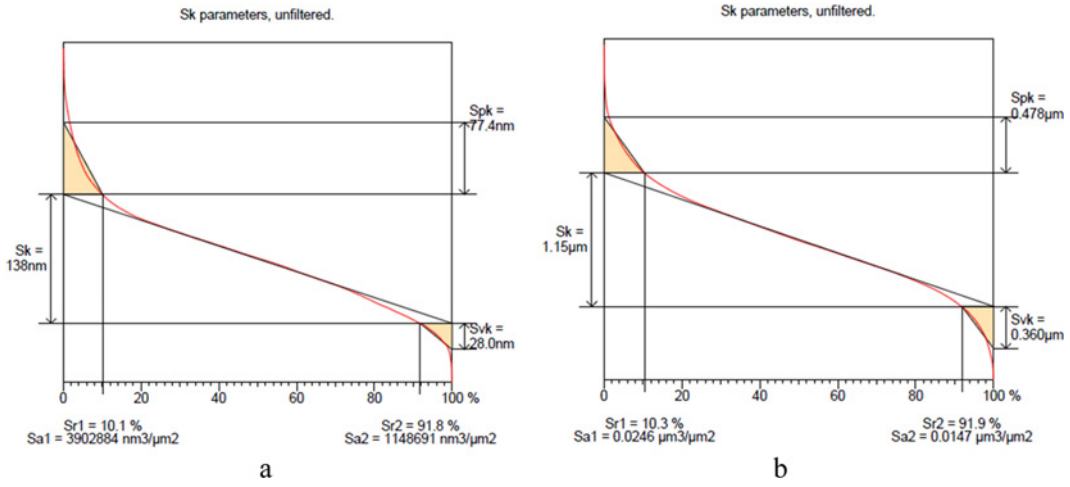

Fig. 9. Graphical study of Sk parameters. The CuTsPc films deposited on glass substrate. a) Scanning square area of 10 μm × 10 μm. b) Scanning square area of 50 μm × 50 μm.

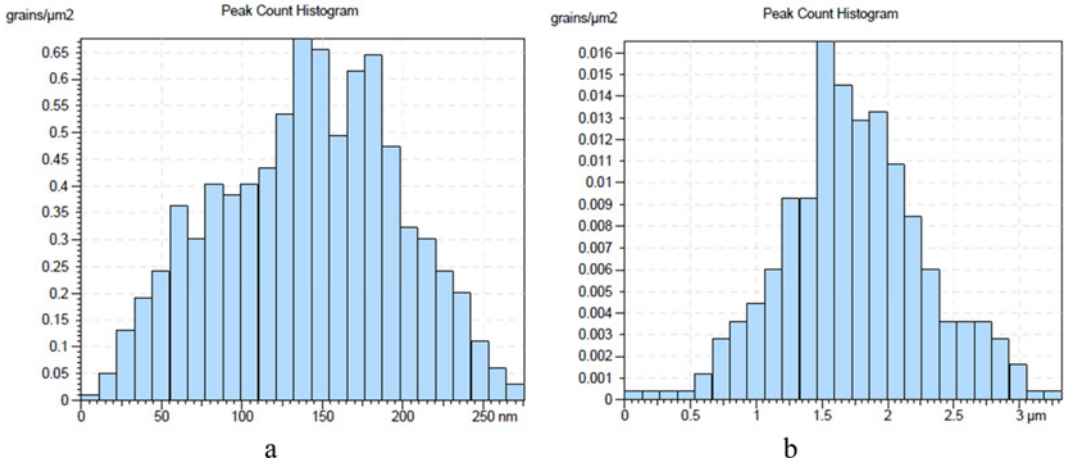

Fig. 10. The peak count histogram. The CuTsPc films deposited on quartz substrate. a) Scanning square area of 10 μm × 10 μm. b) Scanning square area of 50 μm × 50 μm.

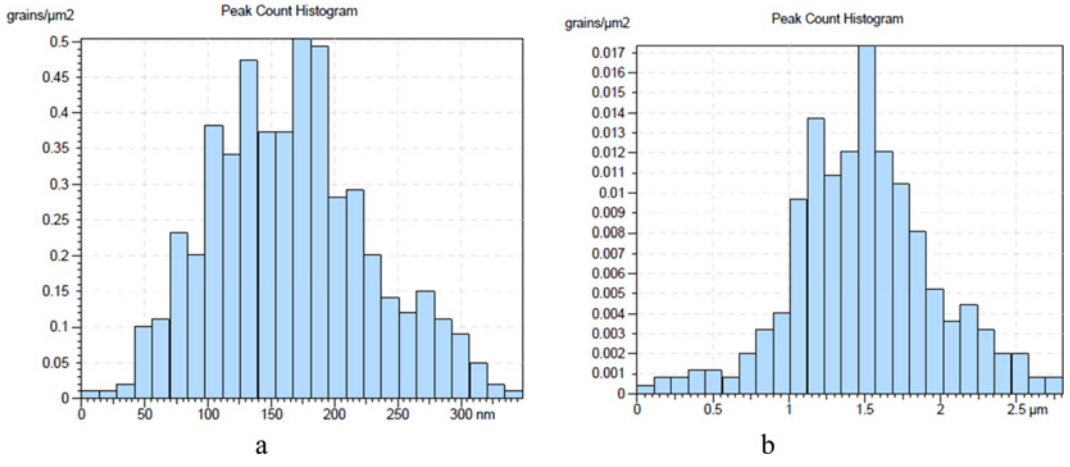

Fig. 11. The peak count histogram. The CuTsPc films deposited on glass substrate. a) Scanning square area of 10 μm × 10 μm. b) Scanning square area of 50 μm × 50 μm.

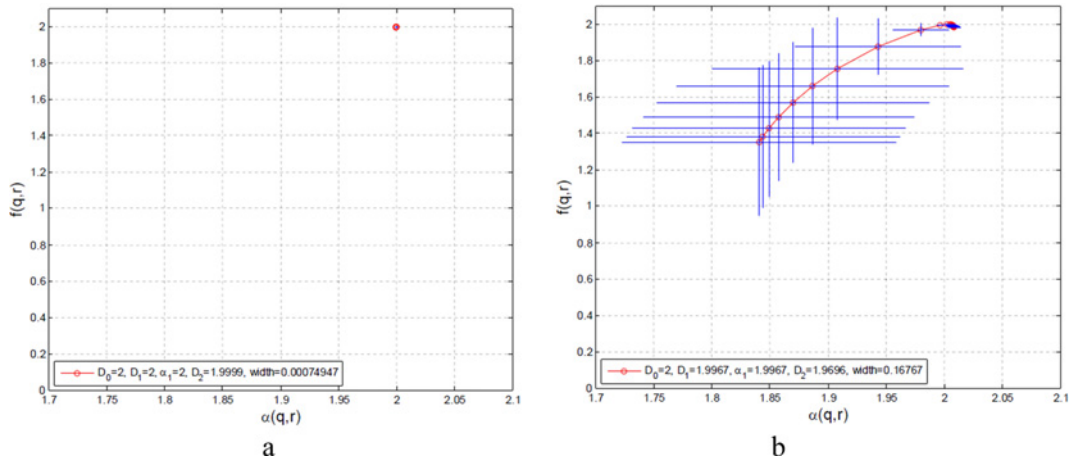

Fig. 12. Multifractal spectrum. The CuTsPc films deposited on quartz substrate. a) Scanning square area of 10 μm × 10 μm. b) Scanning square area of 50 μm × 50 μm.

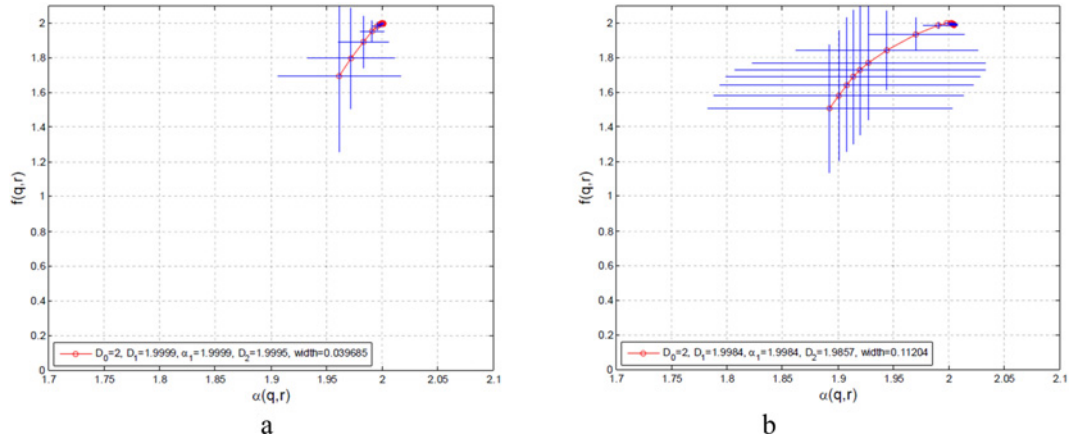

Fig. 13. Multifractal spectrum. The CuTsPc films deposited on glass substrate. a) Scanning square area of 10 μm × 10 μm. b) Scanning square area of 50 μm × 50 μm.

square areas of 10 μm × 10 μm and 50 μm × 50 μm are illustrated in Figs. 12 & 13. The $f(\alpha)$ spectrum was computed in the range $-10 \leq q \leq 10$ for successive 1.0 steps.

It is found that the complexity and roughness of the CuTsPc films increases along with a reduction in the size of the analyzed area. It is also demonstrated that the the CuTsPc films deposited on quartz and glass substrate are multifractal in nature. Strength of the multifractality increases with increasing the analyzed surface area and reducing image detail, whereas it decreases when analyzing a smaller area but with the same resolution (richer in detail). While watching Fig. 2(b) and Fig. 3(b), their similarity can be noticed, which is reflected in the multifractal spectra - Fig. 12(b) and Fig. 13(b). There is a completely different situation when comparing the images for larger magnifications, which is equivalent to the observation of a smaller area with more detail. Fig. 3(a) and particularly Fig. 2(a) seem homogeneous, which is reflected in the multifractal spectrum that for the surface in Fig. 2(a) is reduced to a point (Fig. 12(a)). A similar situation exists when comparing Ssk and Sku parameters (Table 2), which are extremely sensitive to the presence of individual extremes (individual peaks and pits). When comparing Fig. 2(a) and Fig. 3(a) with Fig. 2(b) and Fig. 3(b), it can also be seen that the former ones seem isotropic and the latter ones anisotropic.

Table 1 presents a summary of the generalized dimension D_q values, for the CuTsPc films deposited on quartz and glass substrate, for scanning square area of 100 μm^2 and 2500 μm^2.

A summary of the statistical parameters results of the CuTsPc films deposited on quartz and glass substrate, for scanning square area of 10 × 10 μm^2 and 50 × 50 μm^2, is presented in Table 2.

Table 1. The generalized dimensions (D_q) for q = 0, 1, 2, all with average ± standard deviation, for the CuTsPc films deposited on quartz and glass substrate, for scanning square area of 10 × 10 μm^2 and 50 × 50 μm^2.

No.	Samples	D_0	D_1	D_2	α_1	The spectrum width $\Delta\alpha$
1	Quartz substrate (10 × 10 μm^2)	2.0000 ± 0.00000	2.0000 ± 0.00001	1.9999 ± 0.00004	2.0000 ± 0.00001	0.00074947
2	Quartz substrate (50 × 50 μm^2)	2.0000 ± 0.00000	1.9967 ± 0.00347	1.9696 ± 0.03694	1.9967 ± 0.00347	0.16767
3	Glass substrate (10 × 10 μm^2)	2.0000 ± 0.00000	1.9999 ± 0.00007	1.9995 ± 0.00035	1.9995 ± 0.00007	0.039685
4	Glass substrate (50 × 50 μm^2)	2.0000 ± 0.00000	1.9984 ± 0.00211	1.9857 ± 0.02055	1.9984 ± 0.00211	0.11204

*Statistically significant difference: $P < 0.05$.

Table 2. The statistical parameters of the CuTsPc films deposited on quartz and glass substrate, for scanning square area of 10 × 10 μm^2 and 50 × 50 μm^2.

The statistical parameters	Symbol	Quartz substrate		Glass substrate	
		10 × 10 μm^2	50 × 50 μm^2	10 × 10 μm^2	50 × 50 μm^2
Height Parameters					
Root mean square height	Sq [nm]	55.7	457	54.0	436
Skewness	Ssk [–]	-0.0593	0.309	0.565	0.218
Kurtosis	Sku [–]	2.34	3.19	3.56	2.96
Maximum peak height	Sp [nm]	157	2130	229	1710
Maximum pit height	Sv [nm]	130	1320	135	1210
Maximum height	Sz [nm]	287	3460	363	2920
Arithmetic mean height	Sa [nm]	45.8	363	42.5	349
Functional Parameters					
Areal material ratio	Smr [%]	100	1.20	100	6.35
Inverse areal material ratio	Smc [nm]	73.6	581	66.6	568
Extreme peak height	Sxp [nm]	107	811	88.8	798
Spatial Parameters					
Auto-correlation length	Sal [μm]	2.14	5.21	1.67	4.44
Texture-aspect ratio	Str [–]	0.434	0.520	0.319	0.512
Texture direction	Std [°]	177°	0.363°	3.49°	0.358°
Hybrid Parameters					
Root mean square gradient	Sdq [–]	0.151	0.752	0.226	0.577
Developed interfacial area ratio	Sdr [%]	1.12	14.7	2.43	10.2
Functional Parameters (Volume)					
Material volume	Vm [$\mu m^3/\mu m^2$]	0.00196	0.0267	0.00392	0.0241
Void volume	Vv [$\mu m^3/\mu m^2$]	0.0756	0.608	0.0705	0.592
Peak material volume	Vmp [$\mu m^3/\mu m^2$]	0.00196	0.0267	0.00392	0.0241
Core material volume	Vmc [$\mu m^3/\mu m^2$]	0.0561	0.413	0.0491	0.387
Core void volume	Vvc [$\mu m^3/\mu m^2$]	0.0701	0.563	0.0661	0.548
Pit void volume	Vvv [$\mu m^3/\mu m^2$]	0.00549	0.0447	0.00438	0.0444
Feature Parameters					
Density of peaks	Spd [$1/\mu m^2$]	1.27	0.0194	0.685	0.0189
Arithmetic mean peak curvature	Spc [$1/\mu m$]	4.16	9.38	2.25	5.39
Ten point height	S10z [nm]	87.2	1570	123	1320
Five point peak height	S5p [nm]	70.2	899	80.8	812
Five point pit height	S5v [nm]	17.0	675	41.9	507
Mean dale area	Sda [μm^2]	0.153	37.7	0.421	52.4
Mean hill area	Sha [μm^2]	0.685	42.6	1.09	34.8
Mean dale volume	Sdv [μm^3]	0.000372	0.689	0.000756	0.853
Mean hill volume	Shv [μm^3]	0.00167	1.50	0.00432	1.68

*Statistically significant difference: $P < 0.05$.

4. DISCUSSION AND CONCLUSION

The representative 3D topographic images of the CuTsPc films deposited on quartz and glass substrate, for scanning square area of 100 μm^2 and 2500 μm^2 are shown in Fig. 2(a) & (b) and Fig. 3(a) & (b). The 3D surface of all the samples is covered by nanoasperities (nano scaled protrusions and cavities which have irregular shapes, different sizes and separations) and a specific distribution due to the preparation processes, which is evident for the entire magnification range. This pattern is a clear indication of the multifractal nature of the real surface. Calculations were performed for each data set in the range $-10 \leq q \leq 10$ in q steps of 1.0. In all of the calculations $D_0 > D_1 > D_2$, indicating that the thin film surface roughness had a tendency towards the multifractal scaling property. A statistically significant difference ($P < 0.05$) was found for all D_q values. Results of the generalized dimensions D_q values are summarized in Table 1.

In the box method described with formulas 1-5, the fractal dimension of the surface will always be equal to 2, regardless of its level of development. In the usual method of counting boxes it is vital whether some part of the analyzed set is in a box. The result is a single fractal dimension. However, in the multifractal analysis based on boxes, the result is a whole spectrum of fractal dimensions (detailed explanations are provided in the section on multifractal analysis).[34-37] The capacitive dimension for these surfaces equal to 2 is a correct result, and the width and shape of the multifractal spectrum further characterize the analyzed surface. The applied method reflected the correct values of the generalized dimensions D_q values for $q = 0, 1, 2$ (all with average ± standard deviation) associated for the surface roughness of the thin films. These D_q values should be taken into account in the surface engineering design of CuTsPc films deposited on quartz and glass substrate.

When the multifractal spectrum is wider then it indicates that we need more fractal dimensions in order to describe the multifractal structure while if the width is small the fractal structure comes closer to a monofractal behavior.

The result of this study is determination 3D surface properties of CuTsPc films on the glass and quartz substrate. Their surface morphologies obtained from AFM images were subjected to statistical and multifractal analysis to quantitatively investigate their structural properties. In addition, the multifractal nature of the CuTsPc films on the glass and quartz substrate was investigated and the generalized dimensions (D_q) used as a quantitative factor to estimate of degree of fractality and understand their 3D roughness structures. The CuTsPc films on the glass and quartz substrate surface of all CLs samples appeared relatively smooth, with very fine nano-asperities spread on the surface due to the preparation processes. Results showed that multifractal spectra which include important surface topography information can also be used to investigate the CuTsPc films on the glass and quartz substrate surface. Our results suggest that the CuTsPc films on the quartz substrate have a more homogenous surface structure than glass surface morphology. We have also demonstrated that the CuTsPc films on the glass and quartz substrate are multifractal in nature. The nano-topography of the CuTsPc films deposited on quartz and glass substrate opens a new avenue for both characterization and direct prediction of surface properties and in studies on electro-physical, mechanical, and thermal properties, from both theoretical and experimental perspectives.

The multifractal analysis in correlation with the AFM data information provides a greater insight into surface roughness quality control and performance of the CuTsPc films deposited on quartz and glass substrate.Multifractal analyses highlight the importance of the choice of the size of the analyzed area while maintaining the same resolution. In our case, we have always obtained AFM images with a resolution of 256 × 256 pixels regardless of the size of the analyzed area.

ACKNOWLEDGEMENTS

One of the author Dinesh Pathak would like to thanks the Ministry of Education, Youth and Sports of the Czech Republic, Project CZ.1.07/2.3.00/30.0021 “Strengthening of Research and Development Teams at the University of Pardubice”, who financially supported him.

AUTHOR CONTRIBUTIONS

A.M., D.P., T.W., A.K. and R.K.B. conceived, designed, and performed the experiments. Ş.Ţ. and S.S. designed and described the multifractal analysis and statistical parameters. S.S. and M. Ţ. performed the statistical data analysis. Ş.Ţ., S.S. and D.P. wrote the manuscript. All named authors have seen and approved the final version of the manuscript.

APPENDIX

The statistical parameters of 3D surface roughness, according with ISO 25178-2:2012 are defined as following.[40]

a) Height parameters are a class of surface finish parameters that quantify the Z-axis perpendicular to the surface.

(Sq) – root mean square height is the standard deviation of the height distribution, or RMS surface roughness.

(Ssk) - Skewness is the third statistical moment, qualifying the symmetry of the height distribution. Negative skew indicates a predominance of valleys, while positive skew is seen on surfaces with peaks.

(Sku) - Kurtosis is the fourth statistical moment, qualifying the flatness of the height distribution. For spiky surfaces, Sku > 3; for bumpy surfaces, Sku < 3; perfectly random surfaces have kurtosis of 3.

(Sp) - Maximum peak height is the height between the highest peak and the mean plane.

(Sv) - Maximum pit height is the depth between the mean plane and the deepest valley.

(Sz) - Maximum height is the height between the highest peak and the deepest valley.

(Sa) - Arithmetical mean height is the mean surface roughness.

b) Functional parameters are calculated from the Abbott-Firestone curve obtained by the integration of height distribution on the whole surface.

(Smr) - Areal material ratio is the bearing area ratio at a given height. Ratio of the area of the material at a specified height *c* (cut level) to the evaluation area. The Smr(c) is expressed as a percentage. For the Smr parameter, the height *c* is counted by default from the mean plane.

(Smc) - Inverse areal material ratio is the height c at which a given areal material ratio p is satisfied. The height is calculated from the mean plane.

(Sxp) - Extreme peak height is the difference in height between q% and p% material ratio. This parameter must be configured with two thresholds entered in %.

c) Spatial parameters describe topographic characteristics based upon spectral analysis. They quantify the lateral information present on the X- and Y-axes of the surface.

(Sal) - Auto-correlation length is the horizontal distance of the autocorrelation function (tx, ty) which has the fastest decay to a specified value s, with $0 < s < 1$. The default value for s in the software is 0.2. This parameter expresses the content in wavelength of the surface. A high value indicates that the surface has mainly high wavelengths (low frequencies).

(Str) - Texture-aspect ratio is the ratio of the shortest decrease length at 0.2 from the autocorrelation, on the greatest length. This parameter has a result between 0 and 1. If the value is near 1, we can say that the surface is isotropic, i.e. has the same characteristics in all directions. If the value is near 0, the surface is anisotropic, i.e. has an oriented and/or periodical structure.

(Std) - Texture direction calculates the main angle for the texture of the surface, given by the maximum of the polar spectrum. This parameter has a meaning if Str is lower than 0.5.

d) Hybrid parameters are a class of surface finish parameters that quantify the information present on the X-, Y- and Z-axes of the surface, i.e. those criteria that depend both on the amplitude and the spacing, such as slopes, curvatures etc.

(Sdq) - Root mean square gradient is the root-mean-square slope of the surface.

(Sdr) - Developed interfacial area ratio is the ratio of the increment of the interfacial area of the scale limited surface within the definition area over the definition area. The developed surface indicates the complexity of the surface thanks to the comparison of the curvilinear surface and the support surface. A completely flat surface will have a Sdr near 0%. A complex surface will have a Sdr of some percents.

e) Functional volume parameters are typically used in tribological studies. They are calculated using the Abbott-Firestone curve (areal material ratio curve) calculated on the surface.

Vm(p)- Material volume is the volume of the material at a material ratio p (in %).

Vv(p) - Void volume is the volume of the voids at a material ratio p (in %).

Vmp - Peak material volume of the scale limited surface is the volume of material in the peaks, between 0% material ratio and a material ratio p (in %), calculated in the zone above c1. Vmp = Vm(p)

Vmc - Core material volume of the scale limited surface is the volume of material in the core or kernel, between two material ratios p and q (in %), calculated in the zone between c1 and c2. Vmc = Vm(q) − Vm(p)

Vvc - Core void volume of the scale limited surface is the volume of void in the core or kernel, between two material ratios p and q (in %), calculated in the zone between c1 and c2. Vvc = Vv(p) − Vv(q)

Vvv - Pit void volume of the scale limited surface is the volume of void in the valleys, between a material ratio p (in %) and 100% material ratio, calculated in the zone below c2. Vvv = Vv(p)

f) Feature parameters are derived from the segmentation of a surface into motifs (hills and dales). Segmentation is carried out in accordance with the watersheds algorithm.

Spd - Density of peaks is the number of peaks per unit area.

Spc - Arithmetic mean peak curvature is the arithmetic mean of the principle curvatures of peaks within a definition area.

S10z - Ten point height is the average value of the heights of the five peaks with the largest global peak height added to the average value of the heights of the five pits with the largest global pit height, within the definition area. S10z = S5p + S5v

S5p - Five point peak height is the average value of the heights of the five peaks with the largest global peak height, within the definition area.

S5v - Five point pit height is the average value of the heights of the five pits with the largest global pit height, within the definition area.

Sda - Closed dale area is the average area of dales connected to the edge at height c.

Sha - Closed hill area is the average area of hills connected to the edge at height c.

Sdv - Closed dale volume is the average volume of dales

connected to the edge at height c.

Shv - Closed hill volume is the average volume of hills connected to the edge at height c.

REFERENCES

1. S. R. Forrest, *Nature* **428**, 911 (2004).
2. K. Xiao, Y. Liu, G. Yu, and D. Zhu, *Appl. Phys. A* **77(3-4)**, 367 (2003).
3. S. S. Brar, A. Mahajan, and R. K. Bedi, *J. Optoelectron. Adv. Mat. - Rapid Communications* **5**, 815 (2011).
4. K. Kudo, D. X. Wang, M. Lizuka, S. Kuriyoshi, and K. Tanaka, *Synth. Met*. **111-112**, 11 (2000).
5. M. Shah, M. H. Sayyad, and K. S. Karimov, *J. Semiconductors* **32**, 1 (2011).
6. N. R. Amstrong, *J. Porphyrins Phthalocyanine* **4**, 414 (2000).
7. R. D. Gould, *Coord. Chem. Rev.* **156**, 237 (1996).
8. S. Schumann, R. A. Hatton, and T. S. Jones, *J. Phys. Chem.* **115**, 4916 (2011).
9. C. G. Claessens, U. Hahn, and T. Torres, *Chem. Rec*. **8**, 75 (2008).
10. A. W. Hain, Z. Liang, M. A. Woodhouse, and B. A. Gregg, *Chem. Rev.* **110**, 6689 (2010).
11. A. Kumar, A. Singh, A. K. Debnath, S. Samanta, D. K. Aswal, S. K. Gupta, and J. V. Yakhmi, *Talanta* **82**, 1485 (2010).
12. K. Kato, N. Watanabe, S. Katagiri, K. Shinbo, F. Kaneko, J. Locklin, A. Baba, and R. C. Advincula, *Jpn. J. Appl. Phys.* **43**, 2311 (2004).
13. X. Luo, L. Xu, B. Xu, and F. Li, *Appl. Surface Sci.* **257**, 6908 (2011).
14. G. Chaidogiannos, F. Petraki, N. Glezos, S. Kennou, and S. Nešpůrek, *Appl. Phys. A* **96**, 763 (2009).
15. R. A. Hatton, N. P. Banchard, V. Stolojan, A. J. Miller, and S. R. P. Silva, *Langmuir* **23**, 6424 (2007).
16. S. Berhanus, F. Tariq, T. Jones, and D. W. McComb, *J. Mater. Chem*. **20**, 8005 (2010).
17. M. A. McLchlan, D. W. McComb, S. Berhanu, and T. S. Jones, *J. Mater. Chem*. **17**, 3773 (2007).
18. H. Gupta, A. Mahajan, and R. K. Bedi, *Ind. J. Pure Appl. Phys.* **46**, 435 (2008).
19. O. P. Jaseentha and C. S. Menon, *J. Matter Sci. Mater Electron.* **19**, 602 (2008).
20. H. Gupta, R. K. Bedi, and A. Mahajan, *J. Appl. Phys*. **102**, 073502 (2007).
21. A. O. Abu-Hilal, A. M. Saleh, and R. D. Gould, *Mater. Chem. Phys.* **94**, 165 (2005).
22. A. Mahajan, A. Kumar, M. Singh, D. Pathak, and R. K. Bedi, *Adv. Mat. - Rapid Communications* **6**, 755 (2012).
23. B. Bhushan, *Principles and Applications of Tribology*, p. 90, 2nd ed., John Wiley & Sons Ltd., USA (2013).
24. R. P. Yadav, S. Dwivedi, A. K. Mittal, M. Kumar, and A. C. Pandey, *Appl. Surface Sci.* **261**, 547 (2012).
25. A. Chaudhari and C.-C. S. Yan, *Appl. Surf. Sci.* **238**, 513 (2004).
26. P. Sahoo, T. Barman, and J. P. Davim, *Fractal Analysis in Machining*, p. 6, Springer-Verlag, Heidelberg, Germany (2011).
27. J. Schmähling, *Statistical Characterization of Technical Surface Microstructure*, p. 7, Ph.D. Thesis, University of Heidelberg, Germany (2006).
28. B. B. Mandelbrot, *The Fractal Geometry of Nature*, p. 58, Freeman W. H., San Francisco, USA (1982).
29. B. N. Persson, O. Albohr, U. Tartaglino, A. I. Volokitin, and E. Tosatti, *J. Phys. Condens Matter*. **17**, R1 (2005).
30. C. Q. Yuan, J. Li, X. P. Yan, and Z. Peng, *Wear* **255**, 315 (2003).
31. C. K. Lee and S. L. Lee, *Heterogen Chem. Rev.* **3**, 269 (1996).
32. S. Talu, *ABAH Bioflux* **4**, 1 (2012).
33. H. Xie, J. A. Wang, and M. A. Kwasniewski, *Int. J. Rock Mech. Min. Sci*. **35**, 19 (1999).
34. S. Stach and J. Cybo, *Mater. Charact*. **51**, 79 (2003).
35. S. Stach, S. Roskosz, J. Cybo, and J. Cwajna, *Mater. Charact.* **51**, 87 (2003).
36. S. Stach, J. Cwajna, S. Roskosz, and J. Cybo, *Mater. Sci. Poland* **23**, 573 (2005).
37. S. Stach, J. Cybo, J. Cwajna, and S. Roskosz, *Mater. Sci. Poland* **23**, 583 (2005).
38. S. Stach, S. Roskosz, J. Cybo, and J. Cwajna, *Mater Charact.* **60**, 1151 (2009).
39. W. Kwaśny, *J. Achievements in Mater. Manuf. Eng.* **2**, 125 (2009).
40. ISO 25178-2, Geometrical product specifications (GPS) - Surface texture: Areal - Part 2: Terms, definitions and surface texture parameters. Available from: http://www.iso.org (last accessed August 30 (2013).
41. Product catalog. Available from: http://www.nanosurf.com/ (last accessed August 30, 2013).
42. Silicon AFM Probes. Available from: http://www.vistaprobes.com (last accessed August 30, 2013).
43. SPIP, The Scanning Probe Image Processor, Denmark, 2013. Available from: http://www.imagemet.com (last accessed August 30, 2013).
44. GraphPad InStat software, version 3.20 (GraphPad, San Diego, CA). Available from: http://www.graphpad.com/instat/instat.htm (last accessed August 30, 2013).